J. Plasma Physics (2008), *vol.* 74, *part* 3, *pp.* 353–360. © 2007 Cambridge University Press
doi:10.1017/S0022377807006952 Printed in the United Kingdom

Neoclassical thermal conductivity in ICP plasma at low pressure

A. P. SMIRNOV[1], W. PARK[2], YA. N. ISTOMIN[3], D. P. KOSTOMAROV[1], E. A. SHEINA[1], A. B. SHMLEV[1], and V. N. VOLYNETS[2]

[1] Department of Computational Mathematics and Cybernetics, Moscow State University, Vorobievy Gory, Moscow 119899, Russia (sap@cs.msu.su)

[2] Mechatronics and Manufacturing Technology Center, Samsung Electronics Co., Ltd., 416 Maetan-3Dong, Suwon City, Kyunggi-do 443-742, Korea

[3] Lebedev Physical Institute, Leninsky Prosp. 53, Moscow 119991, Russia

(Received 16 April 2007 and in revised form 30 October 2007, first published online 10 December 2007)

Abstract. The plasma temperature in a new plasma source shows unusual behaviour at low pressures (about 1 mTorr) and high absorbed powers. In Ar plasma at pressures of about 1 mTorr, the electron temperature shows a pronounced maximum inside an electromagnetic accelerator, which is followed by a rapid drop at the boundary between the accelerator region and the main chamber. In this paper a neoclassical thermo-conductivity model based on the analysis of the electron trajectories is proposed to describe the sharp electron temperature profile. Quantitative agreement of the calculated temperature profile with the experiment is observed.

1. Introduction

Plasma sources play an important role in microelectronics processing in areas such as thin film deposition, etching and surface cleaning. In plasma etching the bias voltage is usually used, which is applied to the wafer to produce a high-energy ion flux. This approach has some disadvantages: the use of the bias in plasma etchers is believed to be one the causes of charging damage [1]. In the case of ion acceleration without the use of in-plasma electrodes the ions are accelerated by the electric field, which is the gradient of the plasma potential. Several research groups have reported the creation of such a gradient of the plasma potential in the divergent region of the magnetic field in the case of helicon discharges [2–4]. In some conditions the formation of the double layer (DL) can occur. The DL is characterized by an abrupt jump of the plasma potential at a very short (less than 1 cm) distance. Ions are accelerated in this potential drop to energies of several electron temperature values. The DL has also been obtained for ICP discharge without the magnetic field in an electronegative gas [5].

An ICP source for ion acceleration without electrodes is being developed now at the Samsung Advanced Institute of Technology. In this device the gradient of the plasma potential is created by the ponderomotive action of electromagnetic fields excited in the plasma by an external RF generator. In this paper we present an

https://doi.org/10.1017/S0022377807006952 Published online by Cambridge University Press

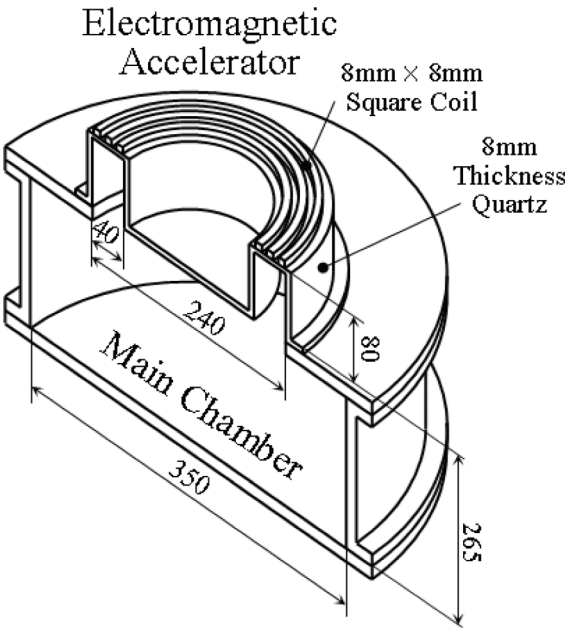


Figure 1. Schematic of the plasma source.

investigation and numerical simulation of ICP plasma at low pressure. At low gas pressure the electron temperature and the plasma potential become larger. So this case is very interesting for ion acceleration. At the same time, at low gas density the electron free path length becomes large compared with the device scale. This determines unusual plasma behaviour [6–10].

2. Experimental setup

Our ICP system [11] as shown schematically in Fig. 1, consists of two main parts: the electromagnetic accelerator (EMA), which is the plasma source, and the main chamber (MC). The EMA consists of two coaxial quartz cylinders with outer diameter 24 cm and the gap between them is equal to 4 cm. The thickness of the quartz walls is 8 mm. Plasma is generated in a 7.5 cm long gap (EMA channel) with a flat three-turn coil placed on the top of the EMA. The coil is powered through the matching box by a 5 kW RF generator with a driving frequency of 2 MHz. The EMA is connected to the stainless steel cylindrical MC with an inner diameter of 35 cm and a height of 26.5 cm. The system is able to produce high-density plasma for a wide range of conditions: gas pressure 0.5–100 mTorr and absorbed power 100–2000 W, which corresponds to a total power of 250–4000 W.

3. Experimental results

All experiments were carried out with Ar gas. Figure 2 shows the experimentally determined electron temperature T_e and plasma density N_e as a function of the axial coordinate z for two pressures, 1.25 and 10 mTorr, and a fixed total RF power of 1800 W. This corresponds to absorbed power values of 840 and 900 W for 1.25 and

https://doi.org/10.1017/S0022377807006952 Published online by Cambridge University Press

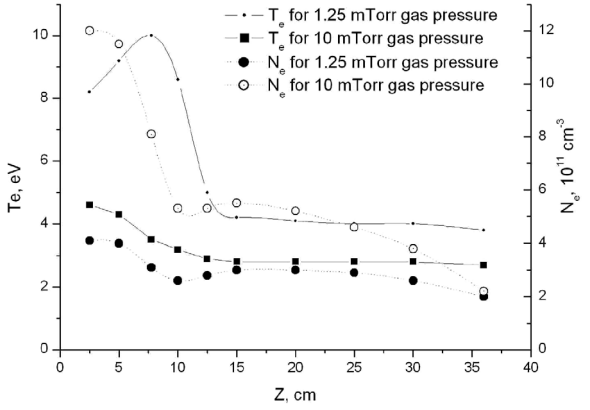


Figure 2. Experimental plasma density and electron temperature.

10 mTorr, respectively. It can be seen from Fig. 2 that the electron temperature and plasma density profiles are quite different for high $\simeq 10$ mTorr and low $\simeq 1.25$ mTorr pressure. Note that $z = 0$ and 36.5 cm correspond to the EMA channel top and MC bottom, respectively, while $z = 7.5$ cm corresponds to the boundary between the EMA and MC.

At high pressure, the absolute values of T_e are moderate, 2.5–4.5 eV; the temperature decreases gradually with z in the EMA channel and is practically constant in the MC volume. Such a behaviour can be considered as normal, as the electron heating takes place mainly in the skin layer close to the top of the EMA. However, the total gradient of T_e is rather high: T_e varies from 4.5 eV near the top of the EMA to about 2.5 eV in the MC volume.

At low pressure, the profile of T_e is quite different and rather unusual. First of all, in the EMA channel T_e is extremely high ($\cong 10$ eV). It shows a maximum in the middle of the channel, followed by a sharp decrease when moving to the MC, and it is much lower ($\cong 4$ eV) in the MC volume. The gradient is highest exactly at the boundary between the EMA and MC.

The plasma density for 10 mTorr is quite high: the maximum value in the EMA channel is $N_e = 1.2 \times 10^{12}$ cm^{-3}, while in the MC volume it is $N_e = 5.5 \times 10^{11}$ cm^{-3}. N_e shows a sharp fall in the channel with increasing z, being almost constant in the MC volume, and then decreases more slowly when approaching the bottom of the MC.

The profile for 1.25 mTorr resembles the high-pressure case, but now the values in the EMA and MC do not differ so much. Moreover, there is a distinct minimum at the boundary between the EMA and MC.

4. Electron dynamics model

Temperature profiles are defined with electron motion:

$$m_e \frac{d\mathbf{v}}{dt} = e\nabla\Phi + \mathbf{F}_{EM} + \mathbf{F}_f, \qquad \frac{d\mathbf{r}}{dt} = \mathbf{v}. \tag{4.1}$$

https://doi.org/10.1017/S0022377807006952 Published online by Cambridge University Press

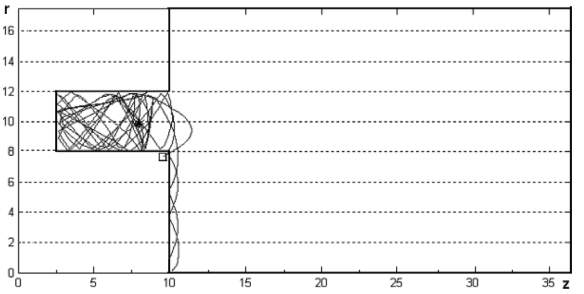


Figure 3. Trajectory of the electron launched inside the EMA at $r_0 = 10\,\mathrm{cm}$, $z_0 = 8\,\mathrm{cm}$.

The ambipolar potential Φ is created by the pondermotive force and the electron pressure

$$\frac{e}{m_\mathrm{e}}\nabla\Phi = \frac{1}{4}\left\{(\widetilde{\mathbf{v}}_\mathrm{e}\cdot\nabla)\widetilde{\mathbf{v}}_\mathrm{e}^{*} + (\widetilde{\mathbf{v}}_\mathrm{e}^{*}\cdot\nabla)\widetilde{\mathbf{v}}_\mathrm{e} + \frac{e}{m}\{[\widetilde{\mathbf{v}}_\mathrm{e}\times\widetilde{\mathbf{B}}^{*}] + [\widetilde{\mathbf{v}}_\mathrm{e}^{*}\times\widetilde{\mathbf{B}}]\}\right\} + \frac{1}{N_\mathrm{e}}\nabla(N_\mathrm{e}T_\mathrm{e}). \qquad (4.2)$$

The forces caused by magnetic and electric fields are $\mathbf{F}_\mathrm{EM} = -e(\mathbf{E} + [\mathbf{v}\times\mathbf{B}])$ and the friction force acting on an electron is $\mathbf{F}_\mathrm{f} = -\nu_\mathrm{coll}\mathbf{v}$, where ν_coll is electron collision frequency; N_e, T_e are electron density and temperature; $\widetilde{\mathbf{B}}, \widetilde{\mathbf{v}}_\mathrm{e}$ are magnitudes of the first harmonic of the magnetic field and electron oscillating velocity. The electromagnetic field magnitudes $\widetilde{\mathbf{E}}, \widetilde{\mathbf{B}}$ are calculated from the Maxwell equations for the first harmonic amplitude, using cold plasma conductivity $\sigma = i\omega_\mathrm{p}^2/4\pi(\omega + i\nu_\mathrm{coll})$. The harmonic electromagnetic fields used in (4.1) are $\mathbf{E} = \widetilde{\mathbf{E}}e^{-i\omega t}, \mathbf{B} = \widetilde{\mathbf{B}}e^{-i\omega t}$.

Wall potential exists at the channel and the camera boundaries. If electron normal energy W does not exceed the sheath value $W_\mathrm{sh} = e\Phi_\mathrm{sh}$, defined by the wall potential Φ_sh, then electrons are reflected. At the glass boundary in the channel the wall potential is determined by the condition of equality of the ion and electron fluxes. This condition gives the following equation for the wall potential:

$$\exp\left(-\frac{e\Phi_\mathrm{sh}}{T_\mathrm{e}}\right) = \left(\frac{e\Phi_\mathrm{sh}}{T_\mathrm{e}}\right)^{1/2}\left(\frac{4\pi m_\mathrm{e}}{m_\mathrm{i}}\right)^{1/2}. \qquad (4.3)$$

Here m_e, m_i are electron and ion masses.

As one can see from the experimental results (Fig. 2), for low gas pressure ($\sim$1 mTorr) discharge electron pressure has a maximal value in the EMA channel. The pressure gradient creates the ambipolar potential well in the EMA. In this case the electrons are trapped in the EMA. Figure 3 shows calculated electron trajectory at a pressure of 1.25 mTorr for the time period between the neighbouring collisions. The electron motions in the radial and longitudinal directions differ significantly. Electrons appearing inside the EMA oscillate in longitudinal direction owing to plasma pressure profile and are reflected from the walls owing to the wall potential. The electron mean free path for our parameters is $l = v\nu_\mathrm{coll}^{-1} \simeq 100\,\mathrm{cm}$. On the other hand, the trapping effect localizes electrons in the longitudinal direction. As a characteristic of this localization we use the standard deviation of the electron position from its mean location in the longitudinal direction. The standard deviation in the longitudinal direction turns out to be much smaller than the mean free path. Figure 4 presents the longitudinal standard deviation along the longitudinal z-axis. In the channel the standard deviation is about 2 cm.

https://doi.org/10.1017/S0022377807006952 Published online by Cambridge University Press

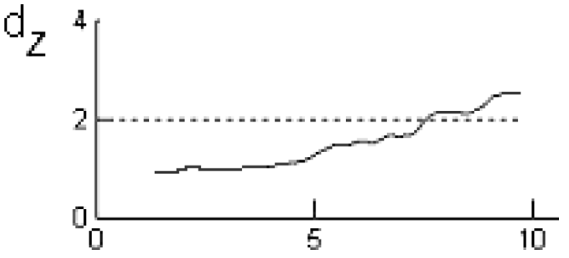


Figure 4. The profile of the standard deviation d of average z-position at the centre of the channel.

The transport coefficients in collision plasma are defined by the mean free path value $l = v_T/\nu_{coll}$, where v_T is the particle thermal velocity. When the value of l is larger than the characteristic scale d of particle motion then the transport coefficients take another form. During the time between the neighbouring collisions $\tau = \nu_{coll}^{-1}$ the particle shifts not by a distance l, but by a distance d. This takes place in a magnetized plasma, when the Larmour radius of the cyclotron rotation of the particle r_c is less than the free path value l, $r_c < l$. In this case the transport coefficients become anisotropic. The transport coefficient along the magnetic field remains as before ($l^2\nu_{coll}$), but the transport coefficient across the magnetic field is defined by the cyclotron radius scale $r_c^2\nu_{coll}$. Furthermore, in a non-uniform magnetic field the magnetized particle moves along the complex drift trajectory, and the size of this trajectory can be less than the free path value l. Such a situation takes place in the magnetic devices for thermonuclear research. In particular, in a Tokamak torus the particle trajectory looks like a banana. The particle diffusion is defined by the banana width d. Such diffusion is called neoclassical diffusion or banana diffusion [12].

In our device, where we have no stationary magnetic field, charged particles move in the high-frequency electromagnetic fields. In this way, they perform complex motion, as we can see from the numerical calculations. The matter is that the Lorenz force $e[\mathbf{v} \times \mathbf{B}]$, acting on the particle, is not small compared with the electric force $e\mathbf{E}$. For the travelling wave, $E \simeq B$ and the Lorenz force is $v/c \ll 1$ times less than the electric force, so we can neglect it. However, we deal with the situation when the device scale is much less than the vacuum wave length $2\pi c/\omega$. The electric field is skinning in this case, $E \propto \exp(-z/\delta)$ (δ is the skin length) and is smaller than the magnetic field, $E \approx (\omega\delta/c)B \ll B$. Thus, if the particle oscillating velocity $\tilde{v} = eE/m\omega$ is large enough, i.e. $\tilde{v} > \omega\delta$, then the Lorenz force becomes larger than the electric force. In this case the particle not only oscillates in the azimuthal direction, but starts moving in the longitudinal direction, along the z-axis. The z-component of the Lorenz force has the quasistationary part, which is the part of the ponderomotive force, and also the part oscillating with the double frequency 2ω (see [9]).

The classic thermal conductivity coefficient is $\kappa = 3.2l^2\nu_{coll}$. In our case the electron oscillates in the z-direction with the scale $d < l$. Therefore, the longitudinal thermal conductivity coefficient $\kappa \approx d^2\nu_{coll}$.

As was previously shown (Fig. 4), the standard deviation of electron oscillations is $d = 2$ cm. So, the longitudinal thermal conductivity coefficient $\kappa_z \approx d^2\nu_{coll}$ in the channel is significantly less than in the MC, $\kappa_z = 3.2l^2\nu_{coll}$. The difference between

https://doi.org/10.1017/S0022377807006952 Published online by Cambridge University Press

these coefficients is about three orders of magnitude. Thus, we can introduce a neoclassical longitudinal thermo-conductivity into our device using the obtained longitudinal standard deviation $\kappa_z = d^2 \nu_{\text{coll}}$.

5. Temperature equation

Electron temperature can be defined as a balance of energy input from the coils and energy losses owing to ionization, temperature flow to the walls, and plasma acceleration. The equation describing the electron temperature has the following form:

$$\frac{3}{2}\left(\frac{\partial T_\text{e}}{\partial t} + \mathbf{V}_\text{e} \cdot \nabla T_\text{e}\right) + T_\text{e} \nabla \mathbf{V}_\text{e}$$

$$= \frac{1}{2N_\text{e}} \text{Re}(\mathbf{j}_\text{e} \mathbf{E}) - \frac{m_i}{2} \mathbf{V}_\text{i} \cdot \nabla V_\text{i}^2 - \frac{m_\text{e}}{2} \mathbf{V}_\text{e} \cdot \nabla \widetilde{v}_\text{e}^2 - \nu_\text{ioniz} W_\text{ioniz} + \nabla(\kappa \nabla T_\text{e}). \quad (5.1)$$

Here the first term on the right-hand side describes energy input, the second term describes losses to ion movement, the third term describes losses to electron movement, the fourth gives the energy losses to ionization and the last term describes thermal conductivity; $\mathbf{V}_\text{e}$ and $\mathbf{V}_\text{i}$ are the slow varying hydrodynamic electron and ion velocity, respectively; $\mathbf{j}_\text{e}$ is the electron oscillating current generated in plasma by the electric field $\mathbf{E}$, $\mathbf{j}_\text{e} = \sigma \mathbf{E}$; $\widetilde{v}_\text{e}$ is the oscillating electron velocity, $\widetilde{v}_\text{e} = -j_\text{e}/en_\text{e}$; ν_ioniz is the ionization frequency; and W_ioniz is the energy of ionization of atoms.

It is worth noting that the nonlinear term proportional to $\nabla \widetilde{v}_\text{e}^2$ in (5.1) and also in (4.1) gives the main contribution to the electron temperature transport and creates the ambipolar potential Φ in the EMA near the coil (more than 90%), but becomes insignificant in MC.

The results of the computation are shown in Fig. 5.

Thus, the whole process can be described in the following way: initially the plasma volume close to the coils is heated. As the thermo-conductivity is low, the temperature is not driven to the large chamber. Convection results in some loss of energy close to the wall $z = 0$ resulting in the maximum being shifted a bit to the middle of the channel. After the temperature reaches high values, it starts penetrating to the chamber, where large thermo-conductivity efficiently spreads it over the whole volume. The value of the ambipolar potential at the metal walls regulates the temperature in the chamber, making it slightly higher than the energy of the electron binding energy in the metal.

The suggested model shows that the two parts of the device, the glass channel and the large chamber, have significantly different plasma parameters and their mutual influence is limited.

6. Conclusion

One can see that even in such a 'simple' device as a plasma source, the physical processes differ greatly from the classical plasma hydro-dynamics description. Electron trajectories have complex forms. They oscillate inside the plasma volume with scales much less that the mean free path. As a result the transport coefficients, in our case the electron thermal conductivity, are significantly less than classical in the longitudinal direction, being huge in the radial direction. This leads to strongly

https://doi.org/10.1017/S0022377807006952 Published online by Cambridge University Press

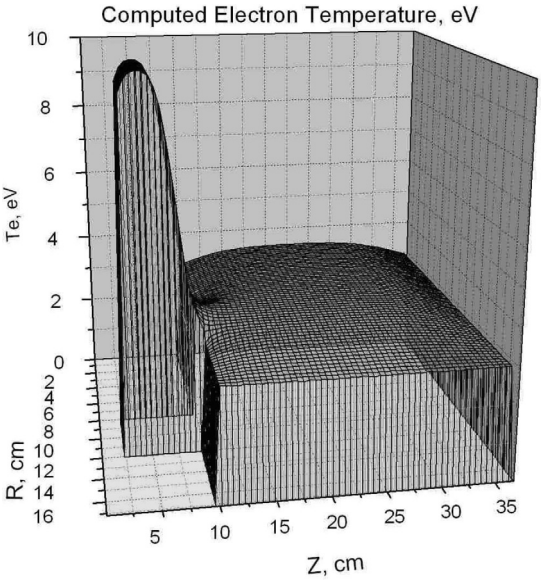


Figure 5. Computed electron temperature. The region with high-temperature gradient corresponds to the region where neoclassical thermo-conductivity becomes classical, which is about three orders of magnitude higher. Radial thermo-conductivity is large everywhere, resulting in uniform temperature for different radii.

anisotropic thermal conductivity. Owing to this the temperature is uniform in the radial direction and has high gradients in the longitudinal direction. The use of such a neoclassical anisotropic thermal conductivity coefficient in numerical simulation shows quantitative agreement with experimental data.

Acknowledgement

This work was supported by Samsung Advanced Institute of Technology.

References

[1] Schaepkens, M. and Oehrlein, G. S. 2001 A review of SiO_2 etching studies in inductively coupled plasmas. *J. Electrochem. Soc.* **148**, C211–C221.

[2] Cohen, S. A., Siefert, N. S., Stange, S., Boivin, R. F., Scime, E. E. and Leninton, F. M. 2003 Ion acceleration in plasmas emerging from a helicon-heated magnetic-mirror device. *Phys. Plasmas.* **10**, 2593–2598.

[3] Charles. C. and Boswell, R. W. 2004 Laboratory evidence of a supersonic ion beam generated by a current-free 'helicon' double-layer. *Phys. Plasmas.* **11**, 1706–1714.

[4] Sun, X., Biloiu, C., Hardin, R. and Scime, E. E. 2004 Parallel velocity and temperature of argon ions in an expanding, helicon source driven plasma. *Plasma Sources Sci. Technol.* **13**, 359–370.

[5] Plihon, N., Corr, C. S. and Chabert, P. 2005 Double layer formation in the expanding region of an inductively coupled electronegative plasma. *Appl. Phys. Lett.* **86**, 091501.

[6] Lieberman, M. A. and Lichtenberg, A. J. 2005 *Principals of Plasma Discharges and Material Processing*, 2nd edn. New York: Wiley.

[7] Vahedi, V., Lieberman, M. A., DiPeso, G., Rognlien, T. D. and Hewett, D. 1995 Analytic model of power deposition in inductively coupled plasma sources. *J. Appl. Phys.* **78**, 1446–1458.

https://doi.org/10.1017/S0022377807006952 Published online by Cambridge University Press

[8] Vasenkov, A. V. and Kushner, M. J. 2002 Electron energy distributions and anomalous skin depth effects in high-plasma-density inductively coupled discharges. *Phys. Rev.* E **66**, 066411.

[9] Godyak, V. 2003 Plasma phenomena in inductively discharges. *Plasma Phys. Control. Fusion* **45**, A399–A424.

[10] Vasenkov, A. V. and Kushner, M. J. 2003 Angular anisotropy of electron distributions in inductively coupled plasmas. *J. Appl. Phys.* **94**, 5522–5529.

[11] Volynets, V. N., Park, W., Tolmachev, Yu. N., Pashkovsky, V. G. and Yoo, J.-W. 2006 Spatial variation of plasma parameters and ion acceleration in an inductively plasma system. *J. Appl. Phys.* **99**, 043302.

[12] Galeev, A. A. and Sagdeev, R. Z. 1968 Transport phenomena in a collisionless plasma in a toroidal magnetic system. *Sov. Phys.–JETP* **26**, 233–240.

https://doi.org/10.1017/S0022377807006952 Published online by Cambridge University Press